

Investigations of Combustion Performance in LPP Combustor

Y. Yan¹, Y. Liu¹, J. Li^{1†} and W. Cai²

¹ Jiangsu Province Key Laboratory of Aerospace Power Systems, Nanjing University of Aeronautics and Astronautics, Nanjing, 210016, China

² School of mechanical engineering, Nanjing University of Science and Technology, Nanjing, China

†Corresponding Author Email: lijinghua@Nuaa.edu.cn

(Received September 4, 2016; accepted April 16, 2017)

ABSTRACT

A Lean Premixed Prevaporized (LPP) low-emission combustor which is applied with the combustion technology of staged lean fuel is developed. To study the cold flow dynamics and the combustion performance of the LPP combustor, both experimental tests using the Particle Image Velocimetry (PIV) to quantify the flow dynamics and numerical simulation using the Fluent software are conducted respectively. To investigate the emissions of the LPP combustor, four kinds of inlet conditions (viz. 7%, 30%, 85% and 100% F_∞ (Thrust Force)) were conducted using numerical simulation. Numerical results are in good agreement with the experimental data. Results show that: 1) a Primary recirculation zone (PRZ), a Corner recirculation zone (CRZ) and a Lip recirculation zone (LRZ) exist in the LPP combustor, and the velocity gradients between pilot swirling flow and primary swirling flow have contributed to the exchanges of mass, momentum and energy. 2) With the decrease of thrust force, NO mass fraction, CO₂ mass fraction and total pressure losses at the exit of LPP combustor fall gradually. 3) Thermal NO formation rate closely relate to the zone area where gas temperature overruns 1900K and the maximum temperature in LPP combustor. 4) The combustion performance of the LPP combustor proposed in this paper is very well, and through comparative analysis with four kinds of typical gas turbine combustor, the NO emission is very low and is equivalent to the CAEP6 43.87%.

Key words: Lean premixed prevaporized (LPP); Low-emission combustor; Cold flow dynamics; Particle image velocimetry (PIV); Combustion performance; NO.

1. INTRODUCTION

As burning fossil fuel, combustion in aircraft engines produce emissions too. A significant proportion of emissions from a jet engine is emitted at a relatively high altitude. These emissions give rise to important environmental concerns regarding their global impact and their effect on local air quality at ground level (Steven *et al.* 2010). Typically, these emissions include oxides of nitrogen (NO_x), carbon monoxide (CO) and unburned hydrocarbons (UHC). Some are classified as hazardous air pollutants (HAPs), and particulate matter (PM) are of concern in the vicinity of airports. NO_x, CO, and UHC emissions from an aircraft and other ground-based sources lead to local and regional production of ozone in photochemical smog reactions while secondary PM precursor gases (NO_x, SO_x, and UHC) can also react in the

atmosphere to form PM. Airborne PM in turn can cause respiratory illnesses and aggravate cardiovascular disease; in addition sulfur also causes acid rain that damages infrastructure. Hence, it is highly desirable to control these emissions through a novel system and components design.

Standards limiting the emissions of smoke, unburned hydrocarbons (UHC), carbon monoxide (CO) and oxides of nitrogen (NO_x) about aero-engine combustors are contained in Annex 16 Volume II to the Committee on Aviation Environment Protection (CAEP) of International Civil Aviation (ICAO). NO_x stringency has subsequently been adopted by CAEP4, CAEP6, CAEP8 in 2004, 2008 and 2010 respectively.

In order to reduce the pollutant emissions, multiple countries have launched a variety of high efficiency

and low emissions combustor development program, and many approaches were considered, including rich burn-quick mix-lean burn (RQL) combustor (Rizk *et al.* 1926; Randal *et al.* 2007), lean premixed prevaporized (LPP) combustor (Lefebvre 1998, Mularz 1979), lean direct injection (LDI) combustor (Fu *et al.* 2007, Yi *et al.* 2009), and so on. In the development of these low emission combustors, the emission performance of aero-engine combustors is directly related to the flow dynamics, the fuel spray characteristics and the fuel/air mixing in the combustion zone of combustor.

Aerodynamic characteristics of the non-reacting, swirling flow field in a lean direct injection (LDI) combustor were investigated by using Particle Image Velocimetry (PIV) (Fu *et al.* 2007) and computational fluid dynamics (CFD) code (Teo *et al.* 2001) respectively. The turbulent flow and flame dynamics within a lean direct fuel injection (LDI) multi-swirler gas turbine combustor were studied by using laser Doppler velocimetry (LDV), particle imaging velocimetry (PIV) and large eddy simulation (LES) (Fureby *et al.* 2007). The flow structure in a Rich burn, Quick quench, Lean burn (RQL) combustor were observed by PIV (Endo *et al.* 2012) and both PIV and a hybrid LES/RANS (Jakirlic *et al.* 2009).

Lean Premixed Prevaporized (LPP) combustors offer one of the best methods to meet the goals of reducing NO_x emissions. Instantaneous vortex and shear layer vortex shedding in a LPP combustor were studied by using PIV, and both non-reacting and reacting conditions were investigated to assess the effects of a flame on the flow (Sulabh *et al.* 2008, 2010, Jacob *et al.* 2014). The structural characteristics in a lean premixed swirl-stabilized combustor, including the formation of recirculation zones and vortex interaction on the combustion instability, were experimentally investigated by using PIV and PLIF measurements (Min-Ki *et al.* 2013, Isaac *et al.* 2012, Stopper *et al.* 2010).

In this paper, a single-section combustor which is used with the combustion technology of staged lean fuel is proposed first. Then, the flow field characteristics and combustion performance of the LPP combustor are experimentally and numerically investigated. The simulations yield a consistency with the experimental data, which provides a better understanding of the flow characteristics and combustion performance in the LPP combustor.

2. RESEARCH OBJECT

Emissions of NO_x, UHC, and CO from an aircraft are formed in the combustors and generally fall into two classes: those formed due to high flame temperature

and that due to low flame temperature, the hot spots will increase NO_x emissions while the cold spots tend to increase CO and UHC emissions. In this study, in order to reduce NO_x emission, a Lean Premixed Prevaporized (LPP) combustor which is applied the combustion technology of staged lean fuel is proposed firstly (as shown in Fig.1, Fig.2 and Fig.3). The LPP combustor produces two co-annular swirling jets by pilot and primary swirler respectively. The pilot swirler includes an annular pilot housing with a hollow interior, a pilot fuel nozzle mounted in the housing adapted for dispensing droplets of fuel to the hollow interior of the pilot housing, and a double of concentrically mounted axial swirlers positioned upstream from the pilot fuel nozzle. Each of the axial swirlers has a plurality of vanes for swirling air. Swirling air then mixes with fuel from the pilot fuel nozzle. The Pilot swirler facilitate to produce a spray quality suitable for starting and low-power operation along with the flow field characteristics appropriate for meeting the design requirements for ignition, starting, lean flame stability, combustion efficiency, etc. The primary swirler includes a main housing defined as annular cavity surrounding the pilot housing, multipoint lean direct injection ports for introducing fuel into the cavity, and a swirler positioned upstream from the multipoint fuel injection ports having a plurality of vanes for swirling air through the swirler to mix air and the droplets from the multipoint fuel injection ports. All of the combustor air except cooling air required for the dome and liners passes through the pilot and primary swirler, therefore more than 60 percent air flows into the flame tube via the pilot swirler and the primary swirler. The diffusion combustion mode is applied by the pilot swirling, therefore, the stable combustion flame can be provided for any conditions and forms a stable ignition source. The premixed pre- evaporation combustion mode is used for the primary swirling, it can decrease the flame temperature and avoid the hot spots, and therefore, the NO_x emission can be reduced. These separated zones of pilot and primary swirlers allow staging for high power and low power duty to be achieved in order to optimize the combustion process.

In order to study the cold flow fields and the combustion performance in the LPP combustor, experimental and numerical studies are used respectively. Firstly the cold velocity profiles of different cross sections and a longitudinal section cutting through the center of the combustor ($Z=0$) are obtained by PIV and numerical simulation separately (The cross plane ($X=0$) is located at the exit of the LPP combustor head. The origin is located at the center of swirler outlet), the cold flow dynamics of the LPP combustor are revealed. In order to verify the numerical simulation accuracy of the combustion performance, then the emissions of a specific

condition are measured via an infrared continuous gas analyzer (Siemens U23, Germany) and numerically simulated separately, the numerical and experimental results are compared. Finally, the combustion performance are investigated for different conditions simultaneously by the numerical simulation, and the EINO of the LPP combustor is obtained.

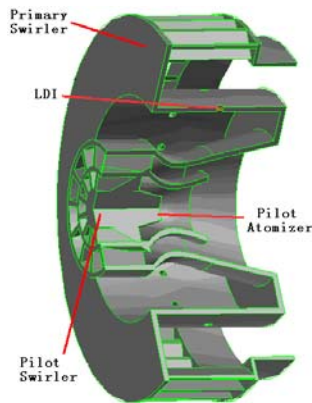


Fig. 1. Structure of LPP low emission combustor head.

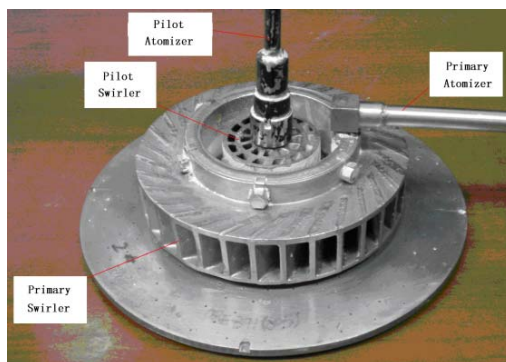


Fig. 2. Photograph of LPP low emission combustor head.

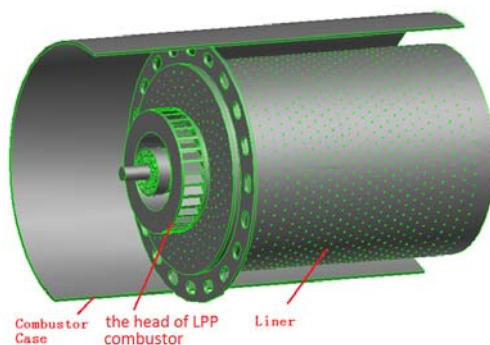


Fig. 3. LPP combustor model.

3. EXPERIMENTAL METHOD

A sketch about the experimental setup for studying the LPP combustor is shown in Fig.4. The

experimental setup includes inlet section, test section, and measuring section of PIV (a multipoint measurement rake is applied for the combustion performance experiment). The compressed air flows through the LPP combustor and the exhaust pipe, then be discharged into the atmosphere. For the cold flow PIV test, the inlet total temperature is 300K, the total pressure is 111458Pa, and the air flow is 0.148kg/s which is metered by an orifice flow meter. For unreactive cold flow experiment, the LPP flame tube is made of quartz glass without cooling holes, and there is an observation window which is put at the end of the measuring section, which is convenient to the PIV measurement; for the combustion performance experiment, the flame tube is made of superalloy with cooling holes.

In order to study the flow dynamics about the LPP combustor, a two-dimensional PIV system of TSI Inc. is used to record the images of the instantaneous velocity patterns, and the average flow field can be obtained by time-averaging algorithm. This PIV system includes a double-pulsed frequency-doubled Nd: YAG laser (200 mJ/pulse at 532 nm) which is used to illuminate the seeding particles, a data acquisition computer, a full resolution of 4 million pixels interline transfer digital CCD camera and a laser-camera synchronizer. The software of TSI Insight 6 is applied for the image acquisition and post-processing. The tracing particle MgO is provided by a seeding generator with a size less than 8 μ m. Such size of the tracing particles ensures that the tracing characteristic and scattering area are optimal at the same time. During the experimental process, more than 250 pairs of instantaneous images can be obtained for every case, then the time-averaged velocity vectors can be gotten by the averaged method of these pairs of instantaneous images.

To verify the prediction accuracy of the numerical simulation for the emissions, the combustion performance experiment of the LPP combustor is conducted at equivalent 100% F_{∞} based on velocity similarity criterion. The inlet total pressure is 2.7MPa, the inlet total temperature is 608K and the fuel air ratio is 0.0242.

To investigate the emissions of the LPP combustor, gas compositions are measured by multipoint measurement rake with water-cooled system. The sampling gas is transmitted to an infrared continuous gas analyzer (Siemens U23, Germany) via a pipe. The pipe is electrically heated to maintain a specific gas temperature based on the CAEP standard requirements.

4. NUMERICAL METHOD

In order to confirm the independence of the mesh, five kinds of mesh are used to calculate the cold flow

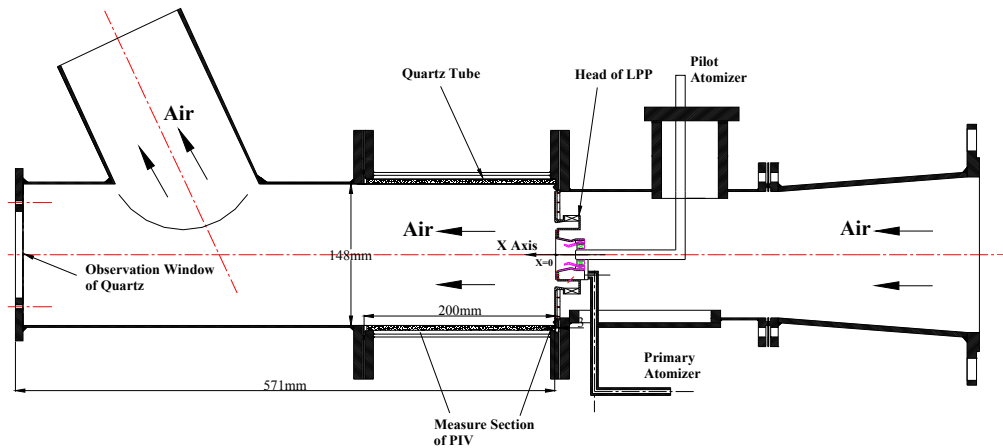


Fig. 4. Sketch of the experimental setup with PIV.

Table 1 Calculation Cases

Case	Take-off	Climb	Landing	Idling
Thrust F_{∞} /KN	100% F_{∞}	85% F_{∞}	30% F_{∞}	7% F_{∞}
Pressure/kPa	3334	2900	1233	459
Temperature/K	839	806	639	511
Excess air coefficient	2.57	2.78	4.07	4.49

field, the numbers of mesh are 1.96 million, 2.7 million, 3.84 million, 4.39 million and 5.21 million respectively. For different kinds of mesh, the velocity magnitude at the same line ($x=50$ and $y=0$) across the combustor are compared as shown in Fig. 5 finally, the mesh number 4.39 million is chosen for the numerical simulation.

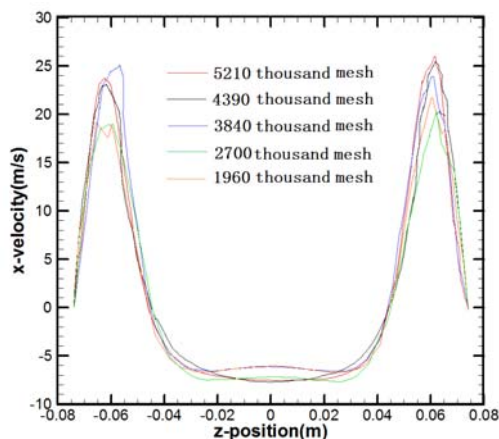


Fig. 5. Verification of mesh independence.

The numerical simulations of the cold flow field and the combustion performance of the LPP combustor are achieved by using FLUENT software. Standard $k-\epsilon$ model is applied to simulate turbulent viscosity. The standard wall function is used to deal with the flow near wall region. For the reactive flow

simulations, the non-premixed equilibrium chemical reaction model and the thermal NO model are applied. The outlet boundary condition is outflow, and inlet conditions of simulation are the same as the experiment settings. The pressure equation is discretized with two order accuracy. The momentum equation, the turbulent kinetic energy equation and the turbulent kinetic energy dissipation rate equation are discretized by using QUICK scheme, and the discrete equations are iterated by using SIMPLE algorithm. For the cold flow simulation, the inlet parameters are the same as the PIV test conditions. And Table 1 shows the inlet conditions for the different combustion performance simulations. When a relative error of flow is less than 5% and all iterative residuals are less than 1.0×10^{-3} , the numerical results are considered to be convergent in this paper.

5. RESULTS AND DISCUSSIONS

5.1 Cold Flow Field Results

Fig. 6 and Fig. 7 show the cold flow field in the LPP combustor by numerical simulation. Fig. 6 is the velocity vector distribution at central plane ($Z=0$). It can be seen that the airflow flows into combustor through pilot swirler, primary swirler and mini cooling holes at the inlets of LPP combustor head. The primary and the pilot swirling jets are co-annular, but the swirling directions are opposite.

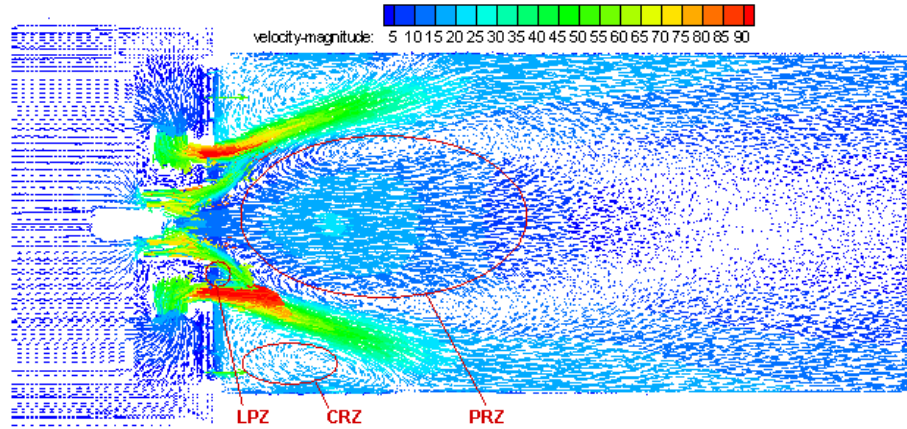


Fig. 6. Velocity vector at central section (Cal.).

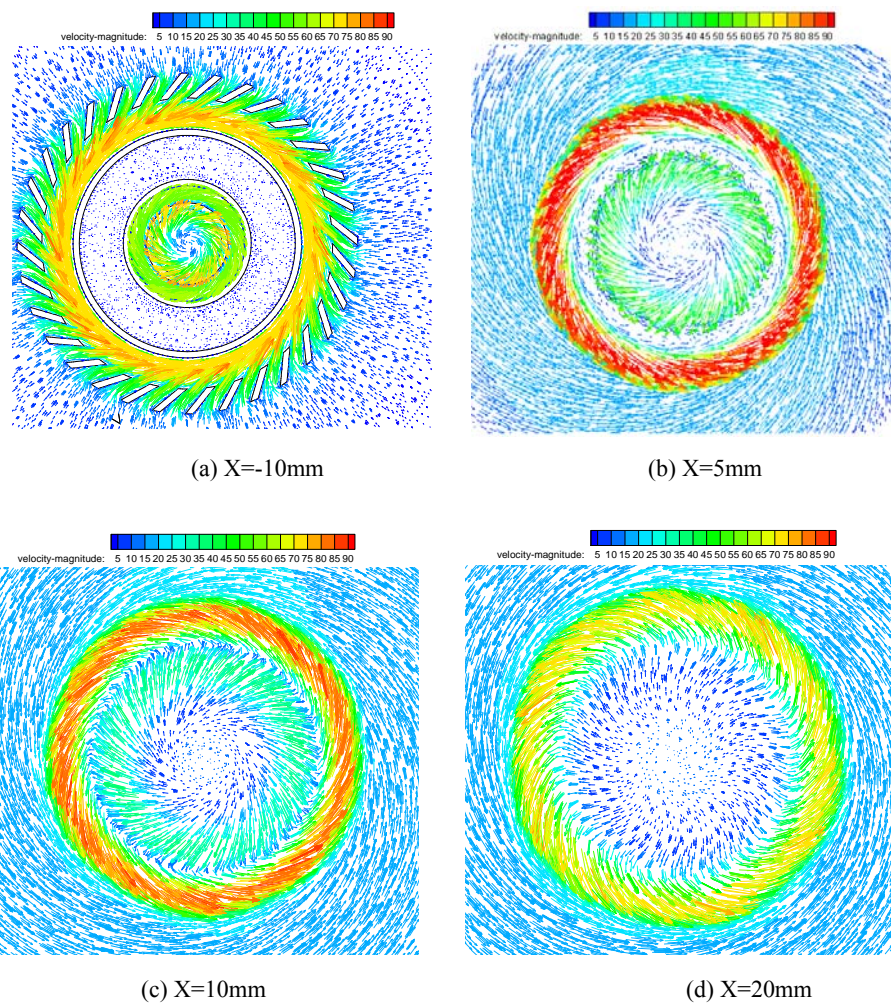


Fig. 7. Velocity vector profiles at different cross sections (Cal.).

Therefore the two co-annular swirling jets can interact with each other, during the moving and interacting process, the two co-annular swirling jets gradually become an annular swirling jet. As shown

in Fig. 9 and Fig. 10, there are axial velocity, vertical velocity and horizontal velocity for these swirling jets at the same time, the swirling jet will gradually expand during the moving and interacting process.

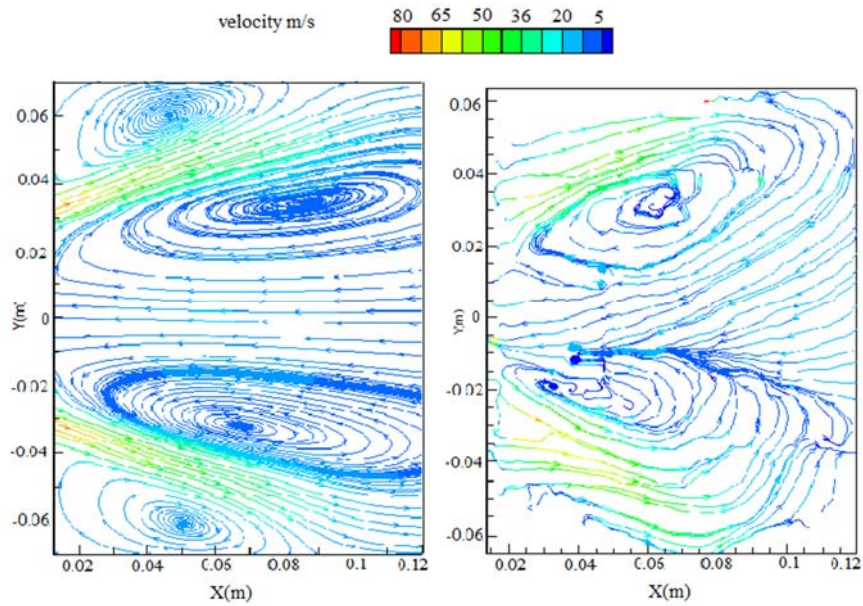


Fig. 8. Partial enlarged plot of velocity streamline at the central section (Cal.(left)&Exp.(right)).

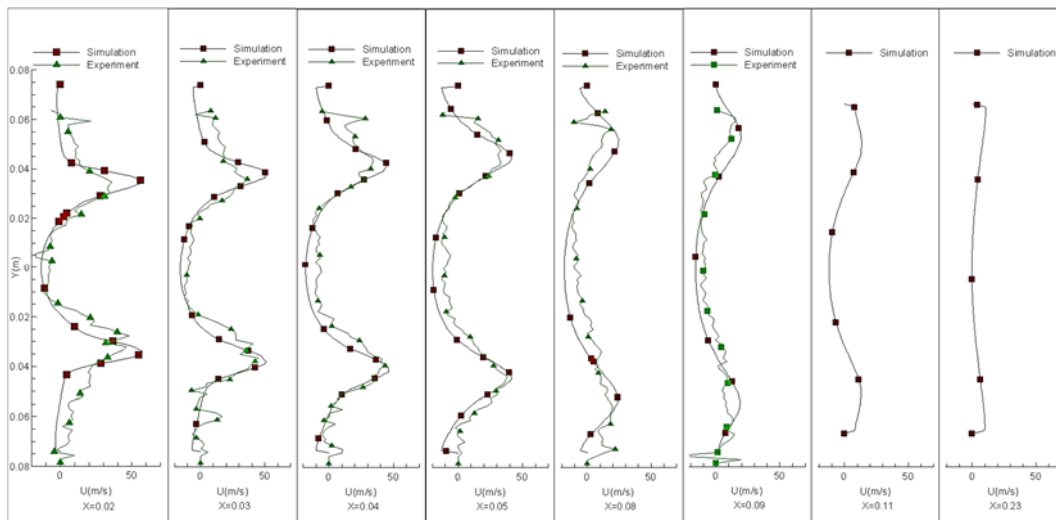


Fig. 9. Radial distribution of the axial velocity at different axial position.

Due to air viscosity, the swirling jets will take the air of central zone away, this can lead to the decrease of the pressure at central zone, then the large radial pressure gradient is formed by the swirling flow. So the Primary Recirculation Zone (PRZ) will be formed because of the low pressure central zone. The PRZ is very important for the flame stabilization. Firstly, the downstream combustion products move forward, at the same time, the heat is also taken to recirculation zone, therefore, it provides a hot zone. The hot gas can accelerate the fuel atomization and ignite the combustible mixed gas, so the recirculated hot gas can act as a stable ignition source. Secondly,

between the recirculation zone and the swirling jet, there is always a reduced velocity region where flow velocity can match the flame speed. Because of the three dimensional structure of swirling jet, the width of PRZ increases with the increase of axial distance firstly, when the width of PRZ reaches a maximum value, then the width of PRZ starts to decrease, finally the PRZ disappears. Because of the sudden expansion in the vicinity of the flame tube head, a Corner Recirculation Zone (CRZ) is provoked, as shown in Fig.6. In addition, there is a smaller Lip Recirculation Zone (LRZ) near the lip of the mixer. This LRZ slows down pilot swirling jet before it

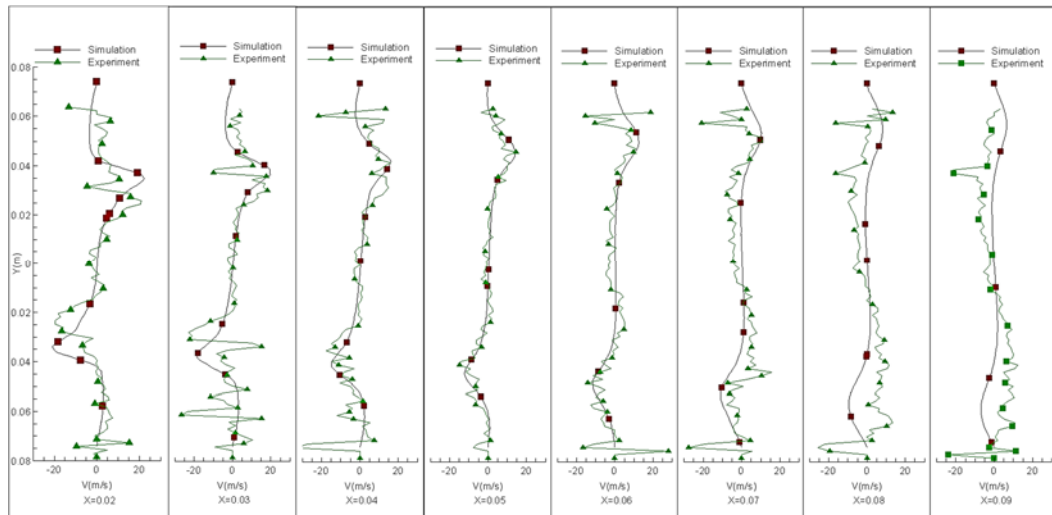


Fig. 10. Radial distribution of radial velocity at different axial position.

merges with primary flow. The LRZ can provide an aid to stabilize the primary flame.

Fig.7 shows the velocity vector profiles at y-z plane with different axial locations ($X=-10, 5, 10, 20\text{mm}$). Figure 7(a) shows the velocity vectors of a cross section at $X=-10\text{mm}$. It is clear that the swirling directions of the rotary jet flows which are injected from the two stage axial pilot swirlers are the same, but is opposite to that of the jet flow from the main radial swirler. Fig. 7 (b) shows the velocity vectors of a cross section at $X=5\text{mm}$. In the pilot swirling jet, the first swirling and the second swirling jets from the two stage axial swirler have the same swirling direction, but swirling speeds are different. As below mentioned of Fig.9, they mix with each other in the venture tube and diffuse outward. Finally they turn into only one pilot swirling jet, but the magnitude of speed decreases. Comparing with Fig. 7 (a), due to the reduced flow area of primary passage, Fig. 7(b) shows that the speed magnitude of primary swirling increases. It can contribute to avoid the presence of flame flash back at the exit of primary swirler. Fig.7(c) shows that there are two co-annular swirling jets which are produced by the pilot swirler and the primary swirler respectively, and the two co-annular swirling jets mixes with each other. Because the air flow rate of the primary swirling jet is much larger than that of the pilot swirling jet, the momentum of the primary swirling jet is far bigger than that of the pilot swirling jet. Therefore, the rotating direction of the pilot swirling jet is finally turned into the rotating direction of the primary swirling jet, during the moving process, the swirling intensity is obviously weakened because of the interaction of the two co-annular swirling jets. Due to the outspread of the annular swirling jet in the radial direction, the width

of the PRZ increases gradually but the velocity magnitude decreases with the increase in the axial distance away from the swirler outlet (e.g. from 10mm to 20mm), as shown in Fig.7 (c) and Fig.7 (d). Fig. 6 and Fig. 7 show that there are exchanges of mass, momentum and energy between pilot swirling and primary swirling due to velocity gradient between these two swirling jets.

Fig.8 shows the partial enlarged plot of velocity streamline at the central section ($Z=0$) from numerical simulation and experiment respectively. Because of the size of the optical window, the starting position for the PIV measurement is 12.5 mm away from the outlet of the swirler. Therefore the LRZ between the pilot swirler and the primary swirler cannot be caught by the PIV. Through the comparative analysis, the experimental results verified the prediction accuracy of the numerical simulation for the cold flow field.

Fig.9 and Fig.10 show the quantitative analysis of the numerical and experimental results, the swirling jet enters into combustor from the swirlers and expands outward. Therefore, the width of the PRZ increases with the increase in axial distance, and the width of the central PRZ reaches maximum when the axial distance is near to 90mm, then the width of the PRZ decreases.

Fig.9 is the radial distribution of the axial velocity at different axial position. It shows that two co-annular swirling jets ejecting from the primary swirler and the pilot swirler has merged into just one swirling jet when the axial distance is over 20mm (as shows in the Fig.7(d)). There are two peaks whose radial positions are around -30mm and 30mm respectively when axial position is 20mm. The two peaks are

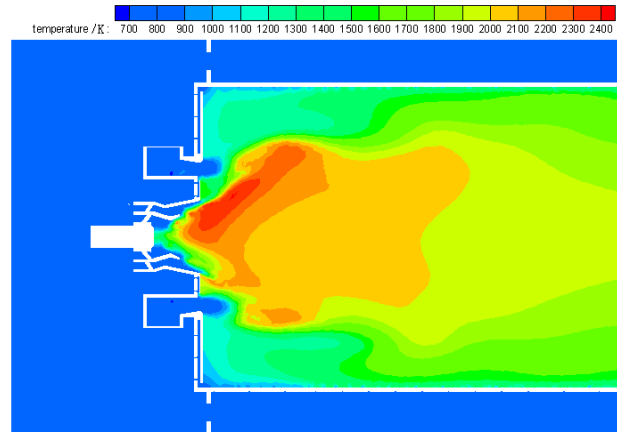


Fig. 11. Contour of temperature at Z=0 pane(100% F_{∞}).

symmetrical with the center line. When the axial distance increases, the swirling jet spreads outside. The width of PRZ increases firstly, and it causes the radial positions of two peaks spreading outward continuously. During the spreading process, the intensity of swirling weakens gradually. Therefore the value of peak decreases. Combing with Fig.8, when the swirling jet gets close to the wall of the combustor, the width of PRZ reaches the maximum. When the axial distance further increases, the width of PRZ decreases gradually until it disappears. It also can be seen that, as the increase of the axial distance, the swirling intensity is weakened, and the radial velocity is decreased, but the radial distributions of velocities are becoming relatively uniform. Through a quantitative analysis, it shows that the numerical results are in good agreement with PIV measurements.

Fig.10 shows the radial distribution of radial velocity at different axial positions. The swirling jet spreads outside, therefore there are one positive radial velocity peak when the radial position Y is above zero and one negative radial velocity peak when the radial position Y is under zero. As the axial distance increases, the position of radial velocity peak increases, but the magnitude of peak decreases. However, the radial distributions of radial velocities become relatively uniform.

Through a quantitative analysis, the numerical results are also in good agreement with PIV measurements. It shows that the turbulent model and numerical simulation methods can be used to simulate the cold flow field of the LPP combustor.

5.2 Combustion Performance Results

Based on the above cold flow dynamics analysis, then the combustion performance of the LPP

combustor is predicted by the FLUENT. In order to calculate the emissions, the CAEP standard specifies a Landing and Take-off (LTO) cycle, including Take-off, Climb, Landing and Idling, they correspond to 100% of total thrust (100% F_{∞}), 85% of total thrust (85% F_{∞}), 30% of total thrust (30% F_{∞}) and 7% of total thrust (7% F_{∞}) respectively, and the corresponding time is 0.7min, 2.2 min, 4.0min and 26min. Four different inlet conditions (viz. 7%, 30%, 85% and 100% F_{∞}) are shown in Table 1. Therefore, these four inlet cases are simulated by the numerical methods, the combustion performance is obtained, such as the temperature distribution, NO_x formation rate, and so on, then, the exit emissions of the LPP combustor can be calculated, finally, the emission index (EI) for the LTO cycle can be gotten based on the calculation formula of CAEP standard.

Fig.11 shows the contours of temperature at Z=0 plane for the 100% F_{∞} . Diffusion combustion mode is applied for the pilot swirling, which leads to higher local fuel concentration, accordingly higher temperature zoon is generated at the outlet of the pilot swirlers. This will contribute to the formation of a stable high temperature ignition source within the flame tube. Multipoint lean direct injectors are used for the primary swirler, meanwhile, the fuel has been completely evaporated and mixed with the primary swirling during the cavity of the primary swiler, therefore, this will lead to the formation of the premixed pre-evaporation combustion mode. So the temperature filed at the outlet of the primary swirler is relative lower and more uniform, it also can be called the detached flame which is stable at a certain distance from the primary swirler outlet, therefore, it is different the diffusion mode at the outlet of the pilot swirler.

NO_x formation rate for 100% F_{∞} is shown in Fig.12.

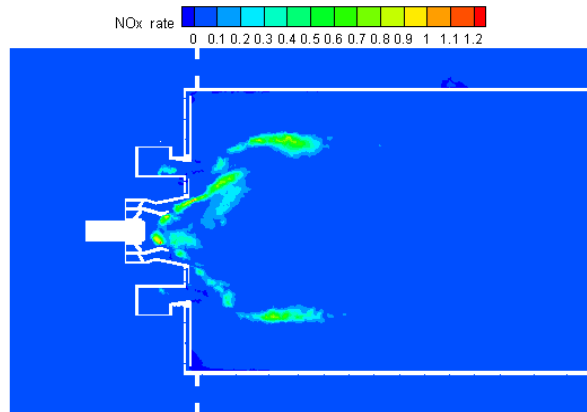


Fig. 12. Contour of NO formation rate at Z=0 plane (100% F_∞).

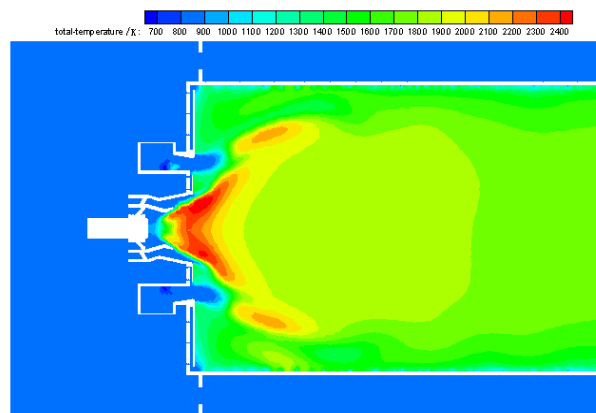


Fig. 13. Contour of temperature at Z=0 plane (85% F_∞).

In gas turbine combustor, nitric oxide (NO) is formed from atmospheric molecular nitrogen (N_2) through three distinct chemical pathways: thermal NO, prompt NO and the N_2O mechanism. For the LPP combustor, the thermal NO mechanism, also referred to as the Zel'dovich mechanism, is the primary formation pathway. Therefore, the high temperature zone size and the maximum temperature determine the thermal NO formation rate. Combining Fig.11 and Fig.12, it is founded that the NOx formation rate corresponds to the temperature distribution. This is because thermal NO formation rate exponentially increase with temperature. When the temperature exceeds 1900K, the thermal NO will generate. As discussed above, diffusion combustion leads to higher temperature more than the premixed pre-evaporation combustion, therefore, the NO formation mainly appear behind the pilot swirler, on the contrary, the NO formation rate is very low behind the primary swirler. To further reduce the NO formation, it is necessary to improve the combustion process behind the pilot swirler.

Figures 13~15 show the temperature distribution at Z=0 plane for different conditions (85% F_∞ , 30% F_∞ and 7% F_∞ respectively). The high temperature zoon basically concentrate behind the pilot swirler. With the decrease of the inlet temperature, pressure and FAR, the maximum of the temperature decreases and the high temperature area also reduces.

Table 2 shows the exit average combustion performance at different cases. With the decrease of the inlet pressure, temperature and FAR, the mass fraction of CO_2 , EINOx and the total pressure loss is on the decrease, while O_2 mass fraction is on the increase. This is because the fuel air ratio decreases, the air involved in combustion is less, so CO_2 mass fraction decreases, and O_2 mass fraction increases. The lower inlet temperature and lower fuel air ratio result in lower temperature and temperature rise, so the thermal NO formation rate is lower. In addition, lower temperature and flow velocity decrease the flow resistance loss and heat resistance loss, separately, so the pressure loss coefficient is on the decrease.

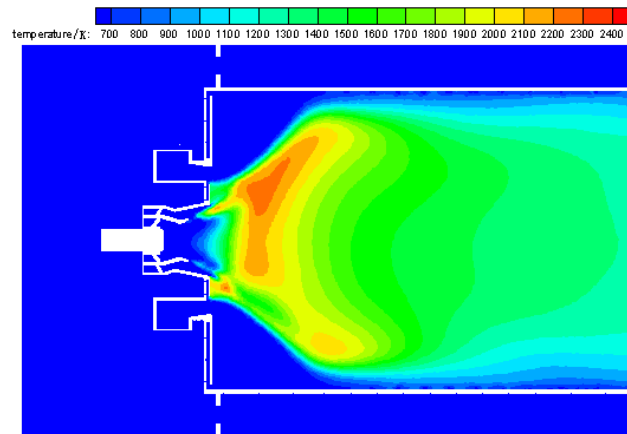


Fig. 15. Contour of temperature at $Z=0$ plane ($7\% F_\infty$).

Table 2 Combustion performance at the outlet of the LPP combustor at different cases

Exit average parameter	O ₂ mass factor	CO ₂ mass factor	EINO(g/kg)	Pressure Loss
100% F_∞	0.1417	0.0794	20.58	5.44%
85% F_∞	0.1473	0.07457	12.06	4.69%
30% F_∞	0.174	0.0513	10.44	4.614%
7% F_∞	0.18	0.0461	6.46	3.76%

Table 3 EINO emission for different combustors

Combustors	Pressure ratio	100% F_∞ (g/kg)	85% F_∞ (g/kg)	30% F_∞ (g/kg)	7% F_∞ (g/kg)	LTO DP/ F_∞ (g/KN)	CAEP6 (%)
LPP combustor	33.3	20.58	12.06	10.44	6.46	28.74	43.84
CFM56-5B3/P	32.8	37.30	28.50	11.20	4.70	58.81	105.7
GE90-76B	35.3	44.86	35.39	12.68	5.88	59.11	90.0
GENx-1B54	35.2	14.96	9.18	8.07	3.98	20.43	34.2

Table 3 shows NO emission for different combustors applied in several typical aero-engines. The four aero-engines have essentially the same pressure ratio. The combustor of CFM56 is typical traditional rich fuel single annular combustor (SAC), the combustor of GE90 is typical dual annular combustor (DAC) and the combustor of GENx is typical twin annular premixing swirler (TAPS) combustor. Table 3 shows that the NO emission of

the LPP combustor proposed in this paper is very low compared to other combustors. Its NO emission is lower than CFM56 and GE90, but is slightly higher than GENx. And the EINO emission of the LPP combustor is equivalent to the CAEP6 standard 43.87%. In summary, the LPP combustor proposed in this paper can greatly reduce the NO emission under the condition of ensuring the other combustion performance.

Table 4 Comparison of LPP exit average combustion performance (Experimental and calculation)

Exit average parameter	Temperature (K)	EINO (g/kg)	Pressure Loss
Calculation	1445	2.845	5%
Experiment	1516	3.05	4.56
Error	4.7%	6.72%	8.8%

In order to verify the simulation accuracy of the combustion model and thermo NO model, experimental investigation and numerical simulation are conducted under the same inlet conditions. Table 4 shows the comparison results, including the outlet average temperature, EINO and total pressure loss. Results show that the experimental results are in good agreement with the numerical results. Therefore, the combustion model and thermo NO model can be used to predict the combustion performance of the LPP combustor.

6. CONCLUSIONS

A LPP Combustor with a staged lean combustion technology was proposed firstly, then the cold flow dynamics and the combustion performance of the LPP combustor are investigated by using experimental and numerical methods. The main results can be summarized as follows:

1. Primary recirculation zone (PRZ), corner recirculation zone (CRZ) and lip recirculation zone (LRZ) are obviously revealed in the cold flow fields of the LPP combustor. The two co-annular swirling jets produced by the pilot and primary swirler respectively interact with each other, therefore, a large radial pressure gradient near the primary swirler exit is generated.
2. The velocity gradients, which are caused by the pilot swirling flow and primary swirling flow, can be clearly observed in the LPP Combustor. The velocity gradients benefit the exchange of mass, momentum and energy between pilot swirling flow and primary swirling flow, and also contribute to the atomization of the fuel and the heat transfer when burning.
3. High temperature zone is formed at the outlet of the pilot swirler because the diffusion combustion mode is applied. This is necessary to form a stable ignite source, but it will promote NO emission.
4. Benefited from multipoint lean direct injectors and well organized flow dynamics, lean, premixed and prevaporized combustion mode is conducted behind the primary swirler. It can

leads to a uniform and relative lower temperature field compared to the traditional diffusion combustion, and this will contribute to lower NO emission.

5. Through comparative analysis with several typical combustor, the NO emission of the LPP combustor is equivalent to the CAEP6 standard 43.87% under the condition of ensuring the other combustion performance .

ACKNOWLEDGMENTS

This work received funding from National Natural Science Foundation of China (No.51676097, 51306092, 91441126).

REFERENCES

- Endo, Y., Y. Yarita, T. Ide, N. Hiromitsu, H. Kawashima and T. Ishima (2012). Evaluation of flow structure in gas turbine combustor models by PIV, *16th Int Symp on Applications of Laser Techniques to Fluid Mechanics*, Lisbon, Portugal 09-12.
- Fureby, C., F. F. Grinstein, G. Li and E. J. Gutmark (2007). An experimental and computational study of a multi-swirl gas turbine combustor, *Proceedings of The Combustion Institute 31*, 3107-3114.
- Jacob, E., P. M. Temme Allison and J. F. Driscoll (2014). Combustion instability of a lean premixed prevaporized gas turbine combustor studied using Phase-averaged PIV, *Combustion and Flame* 161. 958-970.
- Jakirlic, S., B. Kniesner, G. Kavelilil and M. Gnirb (2009). Cameron Tropea, Experimental and computational investigations of flow and mixing in a single-annular combustor configuration, *Flow Turbulence combustion* 83, 425-448.
- Lefebvre, A. H. (1998). *Gas turbine combustion*, Second edition.
- Mularz, E. G. (1979). Lean, premixed, prevaporized combustion for aircraft gas turbine engines,

- AIAA, 1318.
- Rizk, N. K. and H. C. Mongia (1962). Low NOX rich-lean combustion concept application, *AIAA-91*.
- Steven, R. H. Barrett, E. Rex Britter and I. A. Waitz (2010). Global mortality attributable to aircraft cruise emissions. *Environmental Science and Technology*. 44(19).
- Sulabh, K., J. Dhanuka, E. Temme, J. F. Driscoll, M. J. Foust and K. H. Lyle (2010). Unsteady aspects of lean premixed-prevaporized(LPP) gas turbine combustors: flame-flame interactions *AIAA* 1148.
- Sulabh, K. D., J. F. Driscoll and H. C. Mongia (2008). Instantaneous flow structures in a reacting gas turbine combustor *AIAA* 4683.
- Teo, C. Y., Y. K. Siow and S. L. Yang (2001). Flow field study of LDI combustor with discrete jet swirlers using re-stress model *AIAA*.
- Stopper, U., M. Aigner, H. Ax, W. Meier, R. Sadanandan, M. Stohr and A. Bonaldo (2010). PIV, 2D-LIF and 1D-Raman measurements of flow field, composition and temperature in premixed gas turbine flames, *Experimental Thermal and Fluid Science* 34, 396-403.